Langmuir
Article
pubs.acs.org/Langmuir

Shear Thickening in Three Surfactants of the Alkyl Family C_nTAB: Small Angle Neutron Scattering and Rheological Study

J. Dehmoune,[†,§] J. P. Decruppe,*[,†] O. Greffier,[†] H. Xu,[†] and P. Lindner[‡]

[†]*UPV Metz, Laboratoire de Physique des Milieux Denses, ICPM, 1 Bd. D. Arago, Metz F57078, France,* [‡]*ILL Grenoble, Institut Laue-Langevin 6 rue Jules Horowitz, 38000 Grenoble, France, and* [§]*Laboratoire du Futur, Rhodia/CNRS/Université Bordeaux I, 178, avenue du Dr Schweitzer, 33608 Pessac, France*

Received January 22, 2009. Revised Manuscript Received May 13, 2009

Three surfactants of the alkyl family only differing by the length of the aliphatic tail and mixed with sodium salicylate are studied in equilibrium and under flow using rheology and small angle neutron scattering. All three undergo the shear thickening transition associated with the emergence and growth of the so-called shear induced phase or SIS. The rheology in light and heavy water are at first compared, and the influence of the deuterated solvent on the transition characteristics is examined. Small-angle neutron scattering (SANS) experiments are performed on nonflowing solutions in order to find the average cross section radius R_i and the local morphology of the micelles. These data are fitted with two models: a first one that is valid for rigid monodisperse cylindrical particles to get R_i, and a second one that is suitable for semiflexible micelles which shall lead to the contour length L of the micelles. Under flow, scattering experiments are performed over a shear rate range covering three flow regimes. In the first one, prior to the shear thickening transition, the patterns are isotropic; during the last two, corresponding to the existence of the SIS, the scattering figures gradually lose their circular symmetry for an elongated elliptic shape characteristic of an anisotropic medium. The average orientation of the micelles is quantified by the anisotropy factor A_f which turns out to be of the same order of magnitude for the three surfactants.

Introduction

In a steady shear flow, a fluid is said to be shear thickening when its apparent viscosity increases in a well-defined shear rate range. This rheological behavior is quite uncommon, since most of the macromolecular solutions are shear thinning. It is all the more surprising that shear thickening occurs in a concentration domain in which the low shear viscosity of the solution is close to the viscosity of water or at least a few times its value. These solutions belong to the dilute or to the low concentration domain of the semidilute regime. The surfactant concentration is however so small that no one is expecting such unusual behavior.

Since the pioneering experiments of Gravsholt[1] and Hoffman's team,[2,3] the phenomenon is still not fully understood and many studies have tried to tackle it. From all these attempts, general common qualitative features of the initial liquid phase and of the transition come to light:

(i) The surfactant concentration must be smaller or close to the overlap concentration ϕ^*.
(ii) The micelles are asymmetrical and anisotropic, since the solutions already are weakly birefringent before the transition.
(iii) The transition occurs when the shear rate $\dot{\gamma}$ reaches and exceeds a critical value $\dot{\gamma}_c$.
(iv) Even when the shear rate $\dot{\gamma} > \dot{\gamma}_c$, the transition is not instantaneous; a finite induction time is needed prior to the shear thickening to start.
(v) The critical shear rate increases with the temperature.
(vi) Large temporal viscosity fluctuations occur in some solutions.
(vii) The geometry of the shearing device seems to play an important role in the phenomenon.

A large set of experimental techniques is available to investigate the rheophysical properties of the shear induced phase (SIS). Flow birefringence (FB),[4−7] light scattering,[8,9] cryo transmission electron microscopy (cryo-TEM),[7,10] particle image velocimetry (PIV),[11] and small-angle neutron scattering (SANS)[12−16] have been widely used to characterize the flow of shear thickening fluids but also the microstructure of the SIS. Neutron scattering is also well-suited for these studies, and Hayter and Penfold, and Thurn et al.[17,18] were among the first to take advantage of this powerful tool to study the microscopic properties of

*To whom correspondence should be addressed. E-mail: decruppe@univ-metz.fr.

(1) Gravsholt, S. *J. Colloid Interface Sci.* **1976**, *57*, 576.
(2) Rehage, H.; Hoffmann, H. *Rheol. Acta* **1982**, *21*, 561.
(3) Rehage, H.; Hoffmann, H.; Wunderlich, I. *Ber. Bunsen Ges. Phys. Chem.* **1986**, *90*, 1071.
(4) Dehmoune, J.; Decruppe, J. P.; Greffier, O.; Xu, H. *Rheol. Acta* **2007**, *46*, 1121–1129.
(5) Berret, J. F.; Lerouge, S.; Decruppe, J. P. *Langmuir* **2002**, *18*, 7279.
(6) Wunderlich, I.; Hoffmann, H.; Rehage, H. *Rheol. Acta* **1987**, *26*, 532.
(7) Oda, R.; Panizza, P.; Schmutz, M.; Lequeux, F. *Langmuir* **1997**, *13*, 6407.
(8) Liu, C. H.; Pine, D. J. *Phys. Rev. Lett.* **1996**, *77*, 2121.
(9) Boltenhagen, P.; Hu, Y. T.; Matthys, E. F.; Pine, D. J. *Phys. Rev. Lett.* **1997**, *79*, 2359.
(10) Lu, B.; Li, X.; Scriven, L. E.; Davis, H. T.; Talmon, Y.; Zakin, J. *Langmuir* **1998**, *14*, 8.
(11) Hu, Y. T.; Boltenhagen, P.; Matthys, E. F.; Pine, D. J. *J. Rheol.* **1998**, *42*, 1209.
(12) Hoffmann, H.; Hofmann, S.; Rauscher, A.; Kalus, J. *Prog. Colloid Polym. Sci.* **1991**, *84*, 24.
(13) Schmitt, V.; Schosseler, S.; Lequeux, F. *Europhys. Lett.* **1995**, *30*, 31.
(14) Berret, J. F.; Gamez-Gonzales, R.; Oberdisse, J.; Walker, L. M.; Lindner, P. *Europhys. Lett.* **1998**, *41*, 677.
(15) Munch, Ch.; Hoffmann, H.; Ibel, K.; Kalus, J.; Neubauer, G.; Schmelzer, U.; Selbach, J. *J. Phys. Chem.* **1993**, *93*, 4514.
(16) Herle, V.; Kohlbrecher, J.; Pfister, B.; Fischer, P.; Windhab, E. J. *Phys. Rev. Lett.* **2007**, *99*, 158302.
(17) Hayter, J.; Penfold, J. *J. Phys. Chem.* **1984**, *88*, 4589.
(18) Thurn, H.; Kalus, J.; Hoffmann, H. *J. Chem. Phys.* **1984**, *80*, 3440.

micelles under shear. All the results converge toward the same conclusion:

(i) The SIS has a strong anisotropic character revealed by birefringence and neutron scattering.
(ii) Two phases with different viscosities (to be understood as a surfactant rich and a surfactant poor domain[7]) are found in the micellar solution.
(iii) The proportion of the phase with the highest viscosity increases with the shear rate.

Many parameters have been varied: hydrophilic headgroup, length of the aliphatic chain, added salt, concentration of both the salt and the surfactant, temperature, and geometry of the device, but shear thickening still resists all these attempts to understand the origin of this transition.

Apart from the works of Cates and co-workers on the gelation of long micelles and ring driven shear thickening,[19,21] Bandyopadhyay and Sood[20] on rheochaos, Barentin and Liu[22] on the bundle formation at the shear thickening transition, and Olmsted and Lu[23] and Porte et al.[24] on hydrodynamic instabilities, little has been done in the theoretical field.

In this experimental study combining rheology, rheooptics, and SANS, we shall focus on surfactants known to be shear thickening in the dilute and semidilute concentration range. They all are of the alkyltrimethylammonium bromide family and only differ by the length of the aliphatic chain length which contains 14, 16, and 18 carbon atoms. We shall at first compare the rheology in H_2O and D_2O to check the influence of the deuterated solvent on the physical characteristics of the shear thickening transition. In the low shear rate range, they differ by their rheological behavior (shear thinning for C_{18} and C_{16}, Newtonian for C_{14} in D_2O and H_2O.

Then, we will describe SANS experiments at equilibrium and under flow on the same solutions. These results should allow us to characterize the local structure of the micelles (shape, average cross section radius R_i, persistence length l_p, contour length L). We also expect these results to agree with the flow birefringence experiments[4] performed on the same samples and to confirm the idea that the SIS is not destroyed in the shear thinning domain following the shear thickening transition.

Quantitative characterization (radius, flexibility) of the micellar structure has been made on solutions exhibiting shear thickening. These results are correlated for the first time with rheology, flow birefringence, and the evolution of the anisotropy of the micellar structure.

Experimental Section

Materials and Samples. All the solutions under investigation are made up of a surfactant from the alkyl family C_nTAB with an organic salt, the sodium salicylate NaSal. The myristyltrimethylammonium bromide ($C_{14}TAB$ or $CH_3(CH_2)13N(CH_3)^{3+}\ Br^-$) comes from Acros organics, while the cetyltrimethylammonium bromide ($C_{16}TAB$ or $CH_3(CH_2)15N(CH_3)^{3+}Br^-$), the octadecyltrimethylammonium bromide ($C_{18}TAB$, $CH_3(CH_2)$-$17N(CH_3)^{3+}Br^-$), and the NaSal are chemicals from Aldrich Company. They are used as received without any further treatment or purification; the way the solutions are prepared is quite simple: carefully weighted (with a precision of $\pm 10^{-4}$ g) amounts of each surfactant are mixed in distilled water with the necessary amount of NaSal to make equimolar solutions containing 3 mM of each chemical. A concentration of 3 mM is close to the critical micelle concentration (CMC) of C_{14} but well above that for C_{16} and C_{18}. The addition of salt and especially NaSal favors the growth of the micelles and decreases the CMC. This particular surfactant−salt ratio has been found to give the largest amplitude of the shear thickening transition.[25,26] The samples are subjected to the action of ultrasound for a few hours and then left standing still in an oven at 32 °C for at least 3 days prior to any experiments. These solutions which belong to the dilute range of concentration (C_{14}) or are just at the frontier between the dilute and semidilute regime (C_{16} and C_{18}) are not Maxwellian fluids and do not show shear banding prior to the shear thickening transition. The stress relaxation is not monoexponential, and consequently, the three solutions do not relax with a single terminal relaxation time like Maxwellian systems do.

Rheology and Shearing Devices. Two different rheometers are used to study the steady state behavior of the samples: a Rheometric Fluid Spectrometer III (RFS III from TA Instruments) fitted with a 1 mm gap Couette device for the H_2O solutions and a Bohlin apparatus also mounted with a 1 mm cylindrical cell for the samples in heavy water. They are operated in strain controlled mode with the inner cylinder rotating. The geometrical characteristics for the cup and bob, respectively, are as follows: 34−32 mm for the RFS III and 50−48 mm for the Bohlin device. Although the curvature is different, they both have the same gap width, that is, 1 mm. In a typical rheological experimental run to draw the flow curve, the sample is subjected to the action of increasing shear rates and the stress is recorded when the steady state is reached.

Shear thickening is not an instantaneous phenomenon, and a certain shearing time is necessary for the transition to occur. For shear rate values greater than the critical value and for a constant value, the stress increases sharply after an induction period and tends to a constant value: the steady state stress. This induction or incubation time is shear rate dependent, and the lower the shear rate, the longer this induction time. In a previous paper[27] dealing with the kinetics of the transition in the same solutions, we described the way to reach a steady state in these systems prior to recording the stress variations. A shearing time of 600 s for each value of the shear rate is allowed prior to any measurement used to draw the flow curve displayed in Figure 1. For each surfactant, between 6 and 10 values of the shear rate have been chosen in the Newtonian (C_{14}) or shear thinning domain (C_{16} and C_{18}). Thus, the sample is subjected to the shearing for, at least, 1 h before reaching the critical shear rate. This duration is sufficient to reach a steady state for C_{14} and C_{16} but not really for C_{18}. For C_{18}, however, the stress still increases slowly after 10 800 s, but the variation is small and one can rely on the measurements used to draw the flow curve.[27] Thus, we think that the shearing duration in the low shear rate range (before the shear thickening) is large enough to avoid any possible transition at a lower shear rate.

SANS Experiments. The neutron experiments were performed at the Laue Langevin Institute (ILL) in Grenoble on the D11 line. The selected wavelength of the beam was 6 Å with a resolution $\Delta\lambda/\lambda = 10\%$. On that line, the raw data are collected on a 64×64 cm^2 detector which is set parallel to the plane $(\vec{\omega},\vec{v})$. $\vec{\omega}$ lies in the vorticity direction, and $\vec{v}$ defines the direction of the tangential velocity. The sample and the detector were set apart at three distances (2.5, 10, and 36.7 m), thus allowing the wave vector $\vec{k}$ to scan the interval [0.0015−0.15 Å^{-1}]. During the experiments conducted at equilibrium, the samples are subjected to the neutron beam in a standard parallelepipedic quartz cell (1 mm thick). Under flow, the sample fills the above-mentioned Couette

(19) Cates, M. E.; Wang, S. Q.; Bruinsma, R. *Macromolecules* **1991**, *24*, 3004.
(20) Bandyopadhyay, R.; Sood, A. K. *Europhys. Lett.* **2001**, *56*, 447.
(21) Cates, M. E.; Candau, J. S. *Europhys. Lett.* **2001**, *55*, 887.
(22) Barentin, C.; Liu, A. J. *Europhys. Lett.* **2001**, *55*, 432.
(23) Olmsted, P. D.; Lu, C.-Y. D. *Phys. Rev. E* **1997**, *56*, R55.
(24) Porte, G.; Berret, J. F.; Harden, J. L. *J. Phys. II* **1997**, *7*, 459.
(25) Hu, Y.; Rajaram, C. V.; Wang, S. Q.; Jamieson, A. M. *Langmuir* **1994**, *10*, 80.
(26) Hartmann, V. Ph.D. Thesis, Paul Verlaine University, 1997
(27) Dehmoune, J.; Decruppe, J.P.; Greffier, O.; Xu, H. *J. Rheol.* **2008**, *52.4*, 923.

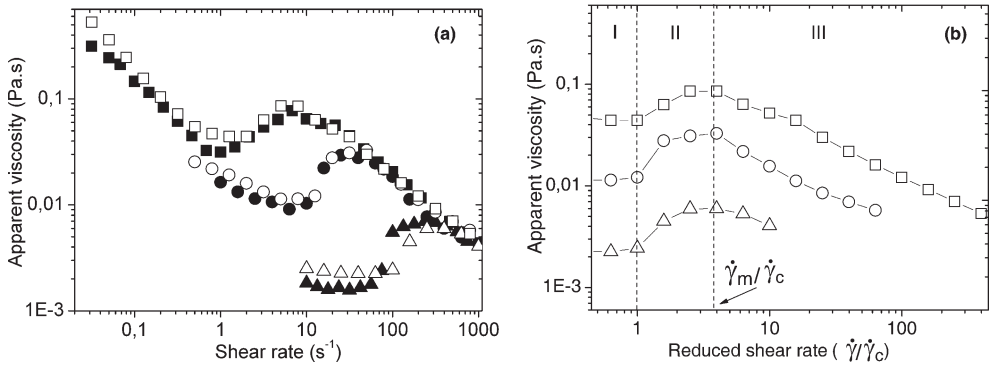

Figure 1. (a) Variation of the apparent viscosity versus the shear rate for the three surfactants C_{18} (□/■), C_{16} (○/●), and C_{14}TAB (△/▲). The empty symbols refer to D_2O, and the full ones to H_2O. (b) Apparent viscosity versus reduced shear rate. Vertical dashed lines drawn at characteristic normalized shear rates values corresponding to the onset of the shear thickening and to the viscosity maximum define three rheological domains in the flow curve of the samples.

device. Two different types of experiments were performed on the three samples; the first one is carried out at rest, while the second type consists of recording the scattered intensity under flow, with the shear rates being mainly chosen in the SIS range. The scattered intensities at equilibrium are at first fitted to a simple cylindrical model to estimate the average radius of the micelles and then to a function which takes the flexibility and the finite length of the micelles into account. Under flow, the scattered intensities in two perpendicular directions (vorticity $\vec{\omega}$ and tangential velocity $\vec{V}$) are used to compute the alignment factor $A_f(q)$, the value of which reflects the average orientation of the micelles under flow.

Prior to any physical interpretation, the raw data have to be normalized and corrected to yield the differential scattering cross section $d\Sigma/d\omega$. We have thus performed all the preliminary measurements necessary to compute the correct cross section. Scattered as well as transmitted intensities through light and heavy water, empty cell, and Cd sheet are recorded and used to correct and normalize the intensity signals.

The scattered pattern collected at the detector is a two-dimensional distribution $I(x,y)$ which is reduced to a single set of data by an averaging process. When the intensity distribution has a circular symmetry (at equilibrium), the data are grouped using the circular averaging procedure on the whole pattern,[28] while, when the pattern is anisotropic (under flow), the averaging is done in an angular sector of 30°; the whole pattern is thus reduced to six series of intensity data, two of which are of particular importance: $I_{\parallel}$ (parallel to the tangential velocity $\vec{v}$) and $I_{\perp}$ (parallel to the vorticity $\vec{\omega}$) which enter the alignment factor $A_f(q)$. All these computations are done with the software written at the ILL.

Results and Discussion

Rheology in H_2O and D_2O. Figure 1a displays the evolution of the apparent viscosity η as a function of the shear rate. The empty symbols refer to D_2O, and the full ones to H_2O. The curves are characteristic of complex fluids undergoing the shear thickening transition which occurs when the shear rate reaches a critical value $\dot{\gamma}_c$. From and after this value, the viscosity increases and reaches a maximum when $\dot{\gamma} = \dot{\gamma}_m$ before decreasing again. The overall qualitative behavior is the same for the three surfactants, with the only difference being a slight shift of the characteristic shear rates ($\dot{\gamma}_c$ and $\dot{\gamma}_m$) toward higher values. Beyond $\dot{\gamma}_m$, the apparent viscosity decreases with the same slope, whatever the length of the aliphatic chain.

The critical shear rate $\dot{\gamma}$ can be used to compute a reduced shear rate $\dot{\gamma}_r = \dot{\gamma}/\dot{\gamma}_c$. Figure 1b shows the variations of the apparent viscosity versus the reduced shear rate. In this new coordinate system (η,$\dot{\gamma}_r$), the emergence of the shear thickening occurs at $\dot{\gamma}_r = 1$ and the reduced shear rate, $\dot{\gamma}_m/\dot{\gamma}_c$, at the viscosity maximum is very nearly the same for the three surfactants.

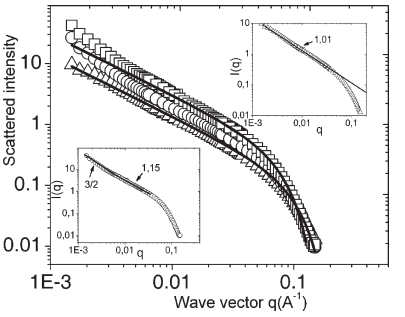

Figure 2. Scattered intensity as a function of the wave vector magnitude q for the three surfactants solutions at the concentration of 3 mM: C_{18} (□), C_{16} (○), and C_{14}TAB (△). The black lines are the graphic representations of eq 1. The small insets in the corners emphasize the behavior of C_{14} (top right) and C_{18} (bottom left); the numerical figures indicate the slope s of a segment considered as linear in a range of wave vectors.

These two particular values of $\dot{\gamma}_r$ can be used to separate the viscosity curve in three domains or regimes corresponding to three different types of rheological behavior of the sample; for $\dot{\gamma}_r < 1$ (regime I), the fluid either behaves similar to a Newtonian liquid or is shear thinning; the second interval, $1 < \dot{\gamma}_r < \dot{\gamma}_m/\dot{\gamma}_c$ (regime II), is the shear thickening domain; and finally, when $\gamma_r > \dot{\gamma}_m/\dot{\gamma}_c$ (regime III), the viscosity decreases again and the fluid is again shear thinning.

SANS at Rest. For each solution, the intensity curve $I(q)$ is built by gathering on a single curve, the data collected at the three sample−detector distances. In Figure 2, the main curves represent, in a log−log plot, the variations of the scattered intensity as a function of the wave vector modulus q for the three surfactants C_{14}, C_{16}, and C_{18} at the concentration of 3 mM. The overall behavior of the three curves is the same: a monotonous decrease with the wave vector q; in the low q range, the three curves are well apart from each other, while in the high q range they nearly superimpose.

The Rigid Monodisperse Particle Model. For N identical rigid particles,[29] the differential scattering cross section writes as

$$\frac{d\Sigma}{d\sigma} = 4\pi^2\phi\Delta\rho^2R^2\frac{1}{q}\left(\frac{J_1(qR)}{qR}\right)^2 \quad (1)$$

(28) Lindner, P.; Zemb, Th. *Neutrons, X-rays and Light. Scattering methods applied to soft condensed matter*; Elsevier Science: North Holland, 2002.

(29) Herbst, L.; Kalus, J.; Schmelzer, U. *J. Phys. Chem.* **1993**, *97*, 7774.

where ϕ stands for the volumic fraction $\phi = NV_p/V$, with N, V_p, and V, respectively, standing for the number of particles of volume V_p in a volume V of solution and $\Delta\rho = \rho_{D_2O} - \rho_{solute}$ for the difference of the scattering length densities.

The local morphology of the micelles can then be deduced from the variations of $I(q)$ in the low q range: for rigid cylindrical particles, we expect a linear variation of $I(q)$ in a log−log plot with a slope = −1 (see eq 1 where $I(q) \propto 1/q$ in the limit $qR \ll 1$). The $1/q$ dependence is well observed all over the low q range ($0.0015 \le q \le 0.022$ Å^{-1}) for C_{14}TAB; C_{16} and C_{18}TAB however do not follow the same pattern in the same q range; the experimental data move apart from the straight line, and the intensity curves show a positive curvature.

The small inset in the top right corner of Figure 2 emphasizes the behavior of C_{14}; a linear fit performed on the experimental data in the range $0.0015 < q < 0.022$ Å^{-1} gives an average slope s of −1.01 as expected in the frame of a rigid cylindrical monodisperse particle model like eq 1. In the bottom left corner, one can follow the variations of $I(q)$ for C_{18}TAB; if the slope s of the curve remains close to −1 in the middle range of q ($0.0045 \le q \le 0.022$, $s = -1.15$), it decreases to −3/2 in the range $0.0015 \le q \le 0.0045$. The same conclusion can be drawn for C_{16}, not represented here.

The micelles in these two solutions already have some degree of flexibility and a finite persistence length l_p for these two surfactants with the longest aliphatic chain length. The simple rigid model is no longer adequate to quantify $I(q)$ over the whole range of wave vectors, and a model which takes the flexibility of the micelles into account has to be introduced. However, for the three surfactants, the experimental distribution agrees with the $1/q$ law in a q range wide enough to conclude that although the micelles of C_{16} and C_{18} have a definite degree of flexibility, the local morphology still remains cylindrical.

The next step consists of calculating the radius of the micelles; to do so, we shall compare the experimental data with the scattering cross section calculated for a group of identical cylindrical micelles in a disordered state. Since no simple model of the structure factor exists for rigid rodlike particles, the comparison shall be restricted to the high q range where $S(q) \simeq 1$.

Gathering all the constants in a single term $A = 4\pi^2\phi\Delta\rho^2$, eq 1 is left with two parameters, A and the cross section radius R_i, readily computed with the help of a nonlinear fitting procedure applied to the experimental data.

The results of the computation procedure appear in Table 1 where the two fitting parameters, that is, the radius R_i with its absolute error ΔR_i and the parameter A, for the three surfactants are listed. The different values of $\Delta\rho$ calculated from A and from the volumic fraction ϕ are added in the same table.

As an element of comparison, Aswal et al.[30] give 22 ± 1 Å for the average radius of a micelle in a 25 mM CTAB/NaSal solution. As expected, the micelle radius increases with the length of the aliphatic chain, and the longer the chain, the larger the radius R_i.

A Model for Flexible Particles. Equation 1 does not hold in the low q range especially for C_{16} and C_{18}TAB; the micelles are no longer rigid cylinders, and the flexibility characterized by a finite persistence length l_p has to be taken into account in the computation. Another way to emphasize the deviation of the experimental data from the theoretical curve is to draw Holtzer's plot $qI(q)$ versus q in a Cartesian coordinates system.[31] In the low q range (see Figure 3), the sudden turning up reveals the flexible structure

Table 1. Fitting Parameters A ($\times 10^{-4}$) and R_i (in Å) with ΔR from SANS Data in the High q Range for the Three Surfactants[a]

	A ($\times 10^{-4}$)	R_i (Å)	ΔR_i	ϕ (%)	$\Delta\rho$ ($\times 10^{10}$ cm^{-2})
C_{18}	2.10	23.4	±0.5	0.117	6.74
C_{16}	1.72	21.0	±0.2	0.109	6.32
C_{14}	1.55	18.6	±0.2	0.1	6.26

[a] The difference of the scattering length densities is calculated from the parameter A and from the volumic fraction ϕ.

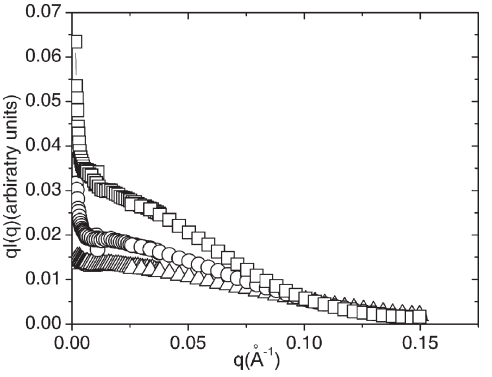

Figure 3. Holzter's plot for the three surfactant solutions at the concentration of 3 mM: C_{18} (□), C_{16} (○), and C_{14}TAB (△).

of the wormlike micelles on a length scale larger than the persistence length.

When the three characteristic lengths of a micelle, that is, L, l_p, and R_i, respectively, the contour length, the persistence length, and the average cross section radius are well apart,[32] the form factor $P(q)$ can be written as the product of two functions $P_{cs}(q,R)$ and $P_{wc}(q,L,l_p)$ and the differential scattering cross section becomes:

$$\frac{d\Sigma}{d\Omega} = \frac{A}{4\pi} R^2 L P(q) \qquad (2)$$

with $P(q) = P_{cs}(q,R)P_{wc}(q,L,l_p)$.

$P_{cs} = \{[2J_1(qR)]/qR\}^2$ is the form factor of a single rigid chain, while $P_{wc}(q,L,l_p)$ stands for that of a wormlike flexible chain of contour length L and persistence length l_p. $P_{wc}(q,L,l_p)$ is a function containing 35 parameters. The description of this function can be found with great detail in the paper by Pedersen and Schurtenberger.[33] The model we are using for the analysis of the data does not take excluded volume effects into account. When $q \gg l_p^{-1}$,

$$P_{ww}(q) \rightarrow P_{rod} = \frac{\pi}{qL}$$

then eq 2 reduces to the scattering cross section of an assembly of rigid particles, that is, eq 1. Owing to this asymptotic behavior, the values of the parameter A and of the cross section radius R_i computed with the rigid particle model (eq 1) can be used in eq 2. A nonlinear fit analysis of the data is then performed over the entire q range with L and l_p as fitting parameters.

The results of the nonlinear fitting session, that is, the contour length L and the persistence length l_p are gathered in Table 2; $I(q)$ is then computed with the help of eq 2 (full line in Figure 4) and compared to the experimental data (open circles). The agreement is excellent over the entire wave vector range up to the upper

(30) Aswal, V. K.; Goyal, P. S.; Thiyagarayan, P. *J. Phys. Chem. B* **1998**, *102*, 2469.
(31) Holtzer, A. *J. Polym. Sci.* **1955**, *17*, 432.
(32) Majid, L. J.; Li, Z.; Butler, P. D. *Langmuir* **2000**, *16*, 10028.
(33) Pedersen, J. S.; Schurtenberger, P. *Macromolecules* **1996**, *29*, 7602.

Table 2. Contour Length L and Persistence Length l_p for C_{16}TAB and C_{18}TAB

surfactant	L (μm)	ΔL (μm)	l_p (Å)	Δl_p (Å)
C_{16}	1.2	0.2	620	20
C_{18}	1.4	0.2	600	20

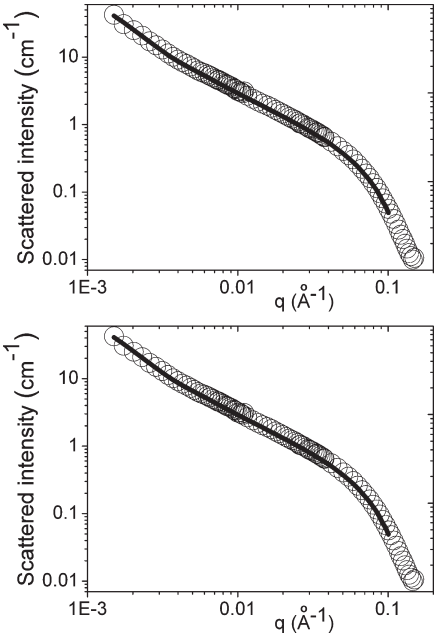

Figure 4. Experimental data (open symbols) and theoretical intensity curve $I(q)$ computed with eq 2 (full black line) for C_{16}TAB (top) and C_{18}TAB (bottom).

bound of 0.1 Å^{-1}. It turns out that the contour length equals 1.2 and 1.4 μm with an error $\Delta L \simeq 0.2$ μm, respectively, for C_{16} and C_{18}TAB; the persistence length is of the same order of magnitude for both surfactants: $l_p = 620 \pm 20$ Å for C_{16}TAB and 600 ± 20 Å for C_{18}TAB. Compared to C_{14}TAB, which fits well with the rigid particle model and consequently has a contour length of the same order of magnitude as the persistence length ($l_p \simeq 260$ Å[34]), the contour length L of C_{16} and C_{18}TAB is surprisingly long; one has to remember that the three samples have the same surfactant concentration, that is, 3 mM, and the cross section radius thus has an important influence on the contour length of the micelles. In the model for semiflexible particles, the structure factor $S(q)$ is also approximate to 1, an assumption which may not be valid any longer for C_{16} and C_{18}TAB and thus leading to an overestimated value of the contour length.

The existence of long wormlike micelles is in agreement with the shear thinning behavior of the C_{16} and C_{18}TAB/NaSal solutions in domain I prior to the shear thickening transition; C_{14}TAB/NaSal however remains Newtonian in the same domain.

To summarize, the results drawn from the SANS data at equilibrium and their physical interpretation show that the micelles are cylindrical with a cross section radius increasing, as one could expect, with the length of the aliphatic chain. The aliphatic chain length thus has an essential role in the micellar growth. Micelles of quite different lengths can lead to shear thickening, and consequently, the initial length at equilibrium of the micelles is not a deciding factor for the shear thickening to occur and has little influence on it.

SANS under Flow. *Regime I:* $\dot{\gamma} \lesssim \dot{\gamma}_c$. The applied shear rate belongs to the range defining regime I but is close to the critical shear rate $\dot{\gamma}_c$ corresponding to the onset of the thickening (see Figure 1). We have chosen the patterns corresponding to 100, 10, and 0.8 s^{-1}, respectively, for C_{14}, C_{16}, and C_{18} to describe the SANS results in the first domain.

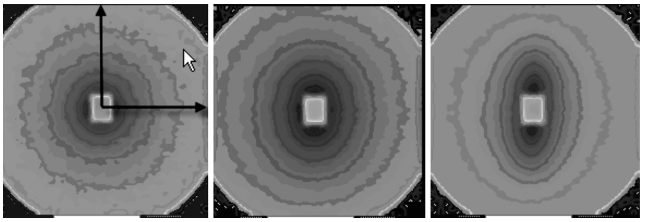

Figure 5. Isointensity contour plot $I(q)$ in the first domain when $\dot{\gamma} \lesssim \dot{\gamma}_c$. From left to right: C_{14} at 100 s^{-1}, C_{16} at 10 s^{-1}, and C_{18} at 0.8 s^{-1}. The vertical and horizontal axes, respectively, define the direction of the vorticity $\vec{\omega}$ and of the tangential velocity $\vec{V}$. The small rectangle near the center is the image of the beam stop. The wave vector $\vec{k}$ scans the interval 0.0015−0.15 Å^{-1}.

Previous flow birefringence experiments[4] performed on the same samples have revealed that the samples already are optically anisotropic in this first domain; the extinction angle which quantifies the average orientation of the micelles is close to zero (direction of the tangential velocity) prior to the viscosity increase, and a small but finite amount of birefringence can already be measured. The SANS data confirm the results of flow birefringence except for C_{14}, the pattern of which still has a circular symmetry for $\dot{\gamma} \lesssim \dot{\gamma}_c$ (see Figure 5). This solution still appears as isotropic for the neutrons when the existence of flow birefringence, although quite weak, implies the existence of a certain degree of anisotropy.

On the contrary, the contour plots of C_{18} have completely lost the circular symmetry; the loci of equal intensity are elongated ellipses stretched in the direction of the vorticity $\vec{\omega}$. This characteristic pattern occurs when the micelles are parallel to the tangential velocity $\vec{V}$.

C_{16} has an intermediate behavior. Moving from the center of the pattern toward the edge, the ellipticity gradually decreases, and, for the largest values of the wave vector, the contour finds its circular shape again. On average and on a short length scale, the solution is isotropic.

The results of flow birefringence[4] indicate that some degree of spatial organization in the micelles of the three surfactants exists before the onset of the shear thickening transition. The SANS isointensity contour plots agree except for C_{14}. One has to remenber that flow birefringence gives a macroscopic view of the degree of optical anisotropy of the sample, typically on a length scale equal to the wavelength of the visible light ($\simeq$0.5 μm). SANS probes the sample on a much smaller scale ($\simeq q^{-1}$). Thus, for the C_{14} solution containing smaller particles, no average order at short distances is detected by the neutrons; this is also the case for C_{16} at large q values where the contour plots are circular.

Regime II: $\dot{\gamma}_c \lesssim \dot{\gamma} \lesssim \dot{\gamma}_m$. For each surfactant, the shear thickening domain is approximately bound by the critical shear rate $\dot{\gamma}_c$ and by $\dot{\gamma}_m$, the shear rate corresponding to the maximum of the viscosity. Three intervals are thus defined: 100−300 s^{-1} for C_{14}, 10−30 s^{-1} for C_{16}, and 0.8−8 s^{-1} for C_{18}. The increasing anisotropy of the samples appears in the scattering patterns which take the shape of ellipses elongated in the vorticity direction $\vec{\omega}$ (see Figure 6, the small patterns associated with the three intensity curves). This particular shape is characteristic of the diffraction pattern given by an assembly of rigid particles all aligned in the same direction, here the direction of the tangential velocity $\vec{V}$. Similar deformations of the SANS patterns have been observed on other shear thickening systems. However,

(34) Shikata, T.; Dahman, S. J.; Pearson, D. S. *Langmuir* **1994**, *10*, 3470.

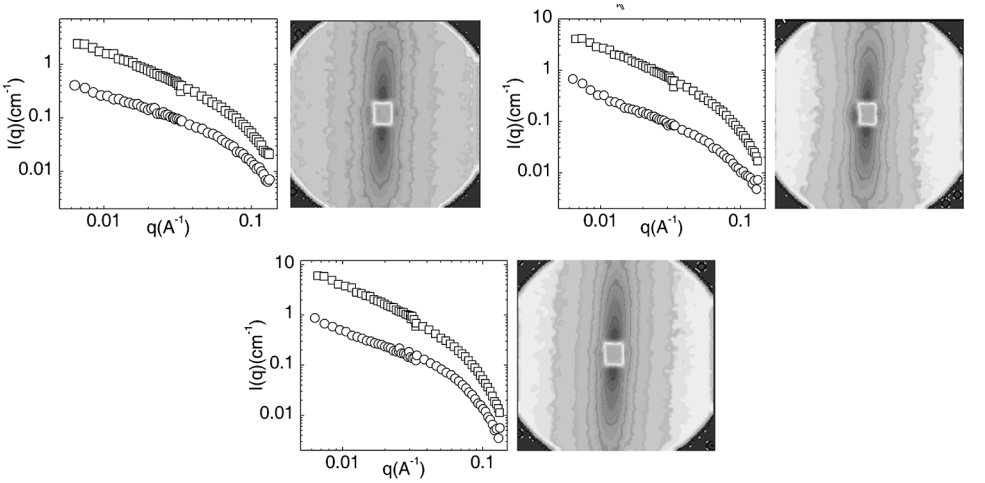

Figure 6. Contour plot and intensity curves $I_{\parallel}(q)$ (○) and $I_{\perp}(q)$ (□) in the shear thickening domain (first domain). From top to bottom: C_{14} at 300 s^{-1}, C_{16} at 30 s^{-1}, and C_{18} at 8 s^{-1}. The pattern in each graph is average in an angular sector of 30° in two perpendicular directions to give $I_{\parallel}$ and $I_{\perp}$. The wave vector $\vec{\kappa}$ scans the interval 0.0015−0.15 $Å^{-1}$.

the concentration of the sample (40 mM) is far from the dilute regime, and the solution is Maxwellian, which is not the case with our systems.[16]

The asymmetrical shape of the patterns also suggests computing the intensity variations in two particular directions: parallel to the tangential velocity $\vec{V}$ (0°) to get $I_{\parallel}$ and to the vorticity $\vec{\omega}$ (90°) for $I_{\perp}$; this is achieved by averaging the distribution in an angular sector 30° wide and centered on the two particular directions: 0° and 90°. For each system and shear rate, the overall qualitative behavior of $I_{\parallel}(q)$ and $I_{\perp}(q)$ is identical to the intensity curve in the first domain (see Figure 2) but they are separate in the vertical direction. In Figure 6, we report, from top to bottom, the variation of $I_{\parallel}$ and $I_{\perp}$ versus the wave vector for the three surfactant systems subjected to the shear rate $\dot{\gamma}_m$: that is, 300 s^{-1} for C_{14}, 30 s^{-1} for C_{16}, and 30 and 8 s^{-1} for C_{18}.

For each shear rate in regime II, the curves $I_{\parallel}$ and $I_{\perp}$ are qualitatively the same; the separation between the two components gradually increases with the shear rate to reach a maximum for $\dot{\gamma} = \dot{\gamma}_m$. In the low q range and under flow, the upturn of $I(q)$ observed at equilibrium and imputed to the flexibility of the micelles disappears in the perpendicular component $I_{\perp}(q)$ while $I_{\parallel}(q)$ still slightly moves away from the straight line: see, for example, $I_{\perp}(q)$ and $I_{\parallel}(q)$ for C_{16} in Figure 6 (second from the top). The strong alignment of the micelles in the direction of the flow by the hydrodynamical field counteracts the thermal agitation; the micelles engaged in the gel-like SIS move less freely, and the flexibility decreases.

Regime III: $\dot{\gamma} > \dot{\gamma}_m$. The shear rate is now chosen in the shear thinning regime following the viscosity maximum. We have already seen[4] that, in this shear rate range, the extinction angle χ remains close to zero and that the birefringence intensity Δn tends to a plateau but surely does not decrease with the shear rate, and consequently, the average orientation of the micelles is in the direction of the flow and the viscosity decrease do not result from a disorganization of the SIS as it has been assumed.[11]

In regime III, the recorded patterns are qualitatively the same as those obtained at the upper boundary of regime II for $\dot{\gamma} = \dot{\gamma}_m$. The micelles forming the SIS keep their average orientation in the direction of the flow.

Figure 7 displays the surface plots in the shear thinning domain for the three surfactants. The isointensity plots (not shown here) all look like elongated ellipsoids. In this last domain, the rheological behavior of the three samples is the same (see the flow curves in Figure 1). The slope is the same, and in the high shear rate range

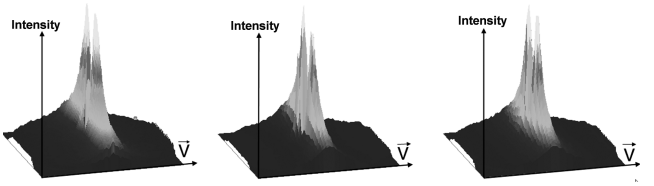

Figure 7. Surface plot of the scattered intensity in regime III. From left to right and top to bottom: C_{14} at 400s $^{-1}$, C_{16} at 100 s^{-1}, and C_{18} at 100 s^{-1}. The wave vector $\vec{\kappa}$ scans the interval 0.0015−0.15 $Å^{-1}$.

($\dot{\gamma} > 600$ s^{-1}) the three solutions have the same apparent viscosity. The length of the aliphatic chain no longer influences the mechanical behavior. On a macroscopic scale, the structure of the SIS is the same for the three surfactants.

Freezed fracture electronic microscopy (FFEM) experiments[37] on equimolar solutions of CTAB/NaSal undergoing the shear thickening transition have revealed the microscopic structure of the SIS. It consists of a spongelike structure rich in micelles embedded in the micellar surroundings. FFEM micropraphs show that their length can reach several micrometers. In such large structures, the dimension of the cross section of the micelle is no longer important, and on a macroscopic scale the three solutions behave in the same manner.

Alignment Factor A_f. The degree of asymmetry of a SANS contour plots is quantified by the alignment factor introduced by Schubert et al.[35] and already used by Herle et al.[16] The integration is performed over a q range identical for the three surfactants and restricted to the small q values ($q \leq 0.03$ $Å^{-1}$).

$$A_f = \frac{\int_{q_a}^{q_b} I_{\perp}(q)\,dq - \int_{q_a}^{q_b} I_{\parallel}(q)\,dq}{\int_{q_a}^{q_b} I_{\perp}(q)\,dq} \qquad (3)$$

where the integration boundaries are $q_a = 0.0015$ and $q_b = 0.03$ $Å^{-1}$.

$A_f = 0$ corresponds to an isotropic medium with no particular orientation. When $A_f = 1$, the alignment in the direction of the flow is fully realized.

(35) Schubert, B.; Wagner, N.; Kaler, E. *Langmuir* **2004**, *20*, 3564.
(36) Decruppe, J. P.; Hocquart, R.; Wydro, T.; Cressely, R. *J. Phys. (Paris)* **1989**, *50*, 3371.
(37) Keller, S. L.; Boltenhagen, P.; Pine, D. J.; Zasadzinski, J. A. *Phys. Rev. Lett.* **1998**, *80−13*, 2725.

Figure 8 displays the variations of the alignment factor A_f versus the reduced shear rate $\dot{\gamma}_r$ for the three surfactants. Again, space can be divided in three domains bounded by two vertical lines, the abscissa of which are the two particular values of the reduced shear rate $\dot{\gamma}_r$ previously introduced (see Figure 1 where the dividing lines are introduced).

The alignment factor A_f of C_{18}TAB remains close to 0.8 ± 0.1 over the entire range of shear rate in the three domains; the micelles of C_{18}TAB already are aligned in the flow direction even under the weakest shearing conditions ($\dot{\gamma} \simeq 0.8\ s^{-1}$), and they keep the same orientation over the entire shear rates range.

For C_{16}TAB and C_{14}TAB, the variations of A_f reflect the change induced by the flow in the micellar arrangement. In the low shear rates range (regime I), $A_f \simeq 0.1$ for C_{14}TAB; the random orientation of the micelles is little influenced by the weak shearing conditions as emphasized by the Newtonian character of the solution. In the same domain, the factor A_f of C_{16}TAB is a slowly increasing function of $\dot{\gamma}_r$, thus showing a gradual orientation of the micelles in the flow in agreement with the shear thinning behavior of the solution.

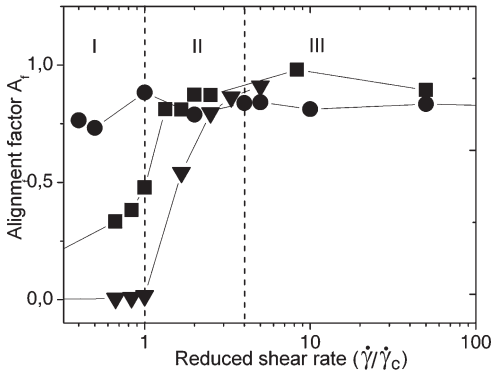

Figure 8. Variation of the alignment factor A_f versus the reduced shear rate for the three surfactants: C_{18} (●), C_{16} (■), and C_{14} (▼). Broken lines define the three regimes introduced in Figure 1.

In regime II, with the emergence and growth of the SIS, both factors increase sharply in a narrow range of shear rates before leveling off to a plateau value of ≃0.8−0.9, which extends in the high shear rates domain (regime III).

Correlation between SANS, Rheology, and Birefringence. Figure 9 gathers the results of the three techniques: neutron scattering (A_f (□)), rheology (apparent viscosity η (▼)), and flow birefringence (extinction angle χ (○) and birefringence intensity Δn (●)). This last optical technique has been described in detail in an earlier paper[36] In order to make the discussion easier, the three regimes (I, II and III) are marked by vertical broken lines.

In regime I, for $\dot{\gamma}$ close to $\dot{\gamma}_c$, a common feature shared by the three solutions is the small value of the extinction angle χ prior to the emergence of the shear thickening. Except for C_{14}, for which χ sharply decreases from 45° in a narrow shear rates range, the extinction angle remains close to a few degrees (≃3−5°) before the viscosity increases. It turns out that a condition necessary for the transition to occur is that the micelles should be organized in an oriented state nearly parallel to the direction of the flow. One can assume that this condition is easily realized, even under weak shearing conditions, for C_{16}TAB and C_{18}TAB considering their contour length. The same argument does not hold for C_{14}TAB; χ close to 45° indicates that the micelles are oriented at random in the flow because of their small geometrical asymmetry. However, as quoted previously in a narrow range of a few s^{-1} below $\dot{\gamma}_c$, χ falls to zero; the micelles have grown in length and orientate in the flow direction. Then the viscosity starts to grow if the shear rate is further increased.

In regime II ($\dot{\gamma}_c \lesssim \dot{\gamma} \lesssim \dot{\gamma}_m$), the angle χ remains close to zero but the birefringence intensity Δn rises to a maximum; since the average orientation of the particles in the direction of the flow is nearly perfect, the increase of Δn can only result from an increase of the proportion of the SIS and not from a better orientation of the particles.

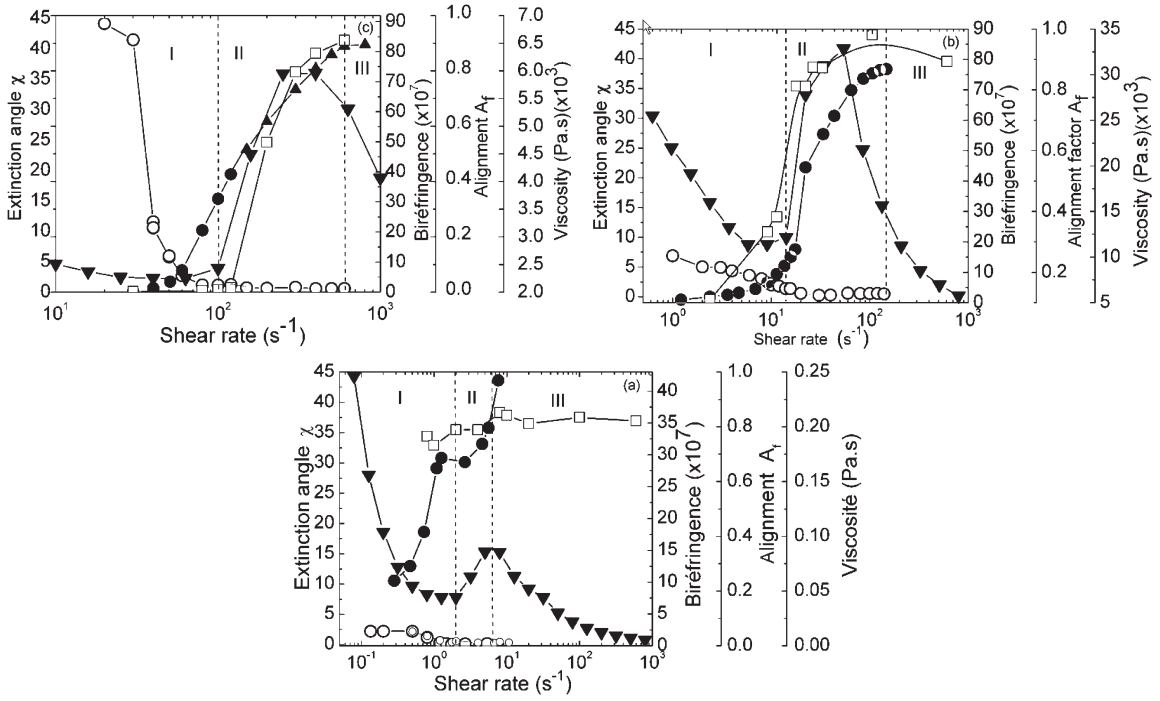

Figure 9. Extinction angle χ (○), birefringence intensity Δn (●), alignment factor A_f (□), and apparent viscosity η (▼) versus the shear rate $\dot{\gamma}$. From top to bottom, C_{14}TAB, C_{16}TAB, and C_{18}TAB. Broken lines define the three rheological domains corrsponding to the three rheological regimes I, II, and III.

Finally, when $\dot{\gamma} > \dot{\gamma}_m$ (regime III), the angle χ remains close to zero and the birefringence as well as the alignment factor A_f level off to a constant value; although the viscosity decreases, the solution keeps a high degree of anisotropy. Consequently, the SIS does not disappear or partly disintegrate but undergoes a structural change which still gives the solution a high degree of anisotropy.

Conclusion

In this work, we have studied and described the shear thickening transition which occurs in three surfactant solutions, with all three belonging to the same family. This choice has the advantage of reducing the number of parameters characterizing the systems; the concentration being the same (3 mM), we are left with the length of the aliphatic tail as the only difference between the samples. We have compared the rheological behavior in strain controlled mode in H_2O and D_2O to find that the nature of the solvent has little influence on the transition, with the critical shear rate $\dot{\gamma}_c$ being just slightly shifted toward higher values.

In the low shear rates range, that is, $\dot{\gamma} < \dot{\gamma}_c$, the samples either behave like a Newtonian fluid (C_{14}) or are shear thinning (C_{16} and C_{18}) in both solvents. The rheological behavior in the low shear rates range is not a deciding factor for the shear thickening transition to occur. Should the micelles be long and entangled or short and nearly free to move, the emergence of the SIS occurs.

From the analysis of the SANS experiments at rest and when a simple rigid particle model is used, we can conclude that the local morphology of the micelles is cylindrical for the three surfactants. In the high q range, the same model leads to the cross section radius R_i of the micelles which is found, as expected, to increase with the length of the aliphatic tail.

In domain I (low q), the intensity curves of C_{16}TAB and C_{18}TAB depart from the straight line in a log−log plot as a consequence of the increasing flexibility of the micelles; we have used the model built by Pedersen and Schurtenberger[33] which takes the persistence length and the contour length into account to fit the data. If the computed values of l_p are in agreement with other data, the contour length is found to be surprisingly long at such a low concentration in surfactant. This really long dimension however explains well the shear thinning behavior of C_{16}TAB and C_{18}TAB prior to the transition, with shear thinning resulting from the orientation of the long micelles in the direction of the flow.